COMPUTATIONAL STUDY OF TURBULENT HEAT TRANSFER FOR HEATING OF WATER IN A SHORT VERTICAL TUBE UNDER VELOCITIES CONTROLLED

K. Hata¹, N. Kai², Y. Shirai², S. Masuzaki³ and A. Hamura⁴

¹ Institute of Advanced Energy, Kyoto Univ., Gokasho, Uji, Kyoto 611-0011, Japan
 ² Dept. of Energy Science and Technology, Kyoto Univ., Sakyo-ku, Kyoto 606-8501, Japan
 ³ National Institute for Fusion Science, 322-6 Oroshi-cho, Toki, Gifu 509-5292, Japan
 ⁴ Concentration Heat and Momentum Ltd., 3-5-4 Koji-machi, Chiyoda-ku, Tokyo 102-0083, Japan

hata@iae.kyoto-u.ac.jp, kai@pe.energy.kyoto-u.ac.jp, shirai@pe.energy.kyoto-u.ac.jp masuzaki@LHD.nifs.ac.jp, hamura@phoenics.co.jp

Abstract

The steady-state turbulent heat transfer coefficients in a short vertical Platinum (Pt) test tube for the flow velocities (u=4.11, 7.12, 10.07, 13.62, 21.43, 30.72 and 41.07 m/s), the inlet liquid temperatures (T_{in} =296.47 to 310.04 K), the inlet pressures (P_{in} =810.40 to 1044.21 kPa) and the increasing heat inputs ($Q_0 exp(t/\tau)$, exponential periods, τ , of 6.04 to 23.66 s) were systematically measured by an experimental water loop comprised of a multistage canned-type circulation pump with high pump head. Measurements were made on a 59.2 mm effective length and its three sections (upper, mid and lower positions), which were spot-welded four potential taps on the outer surface of the Pt test tube of a 6 mm inner diameter, a 69.6 mm heated length and a 0.4 mm thickness. The outer surface temperature distribution of the Pt test tube was also simultaneously observed by an infrared thermal imaging camera at intervals of 3 seconds.

Theoretical equations for turbulent heat transfer in a circular tube of a 6 mm in diameter and a 636 mm long were numerically solved for heating of water with heated section of a 6 mm in diameter and a 70 mm long by using PHOENICS code under the same condition as the experimental one considering the temperature dependence of thermo-physical properties concerned. The surface heat flux, q, and the surface temperature, T_s , on the circular tube solved theoretically under the flow velocities, u, of 4.11, 7.12, 10.07, 13.62, 21.43, 30.72 and 41.07 m/s were compared with the corresponding experimental values on heat flux, q, versus the temperature difference between heater inner surface temperature and liquid bulk mean temperature, ΔT_L [= T_s - T_L , T_L =(T_{in} + T_{out})/2], graph. The numerical solutions of q and ΔT_L are almost in good agreement with the corresponding experimental values of q and ΔT_L with the deviations less than ± 10 % for the range of ΔT_L tested here. The numerical solutions of local surface temperature, $(T_s)_z$, local average liquid temperature, $(T_{f,av})_z$, and local liquid pressure drop, ΔP_z , were also compared with the corresponding experimental data on $(T_s)_z$, $(T_{f,av})_z$ and ΔP_z versus heated length, L, or distance from inlet of the test section, Z, graph, respectively. The numerical solutions of local surface temperature, $(T_s)_z$ and local average liquid temperature, $(T_{f,av})_z$ are within ± 10 % of the corresponding experimental data on $(T_s)_z$ and $(T_{f,av})_z$, although those of local liquid pressure drop, ΔP_z , become 37.6 % lower than the experimental ones. The thickness of the viscous sub-layer, δ_{VSL} [=(Δr)_{out}/2], and the non-dimensional thickness of

viscous sub-layer, $y^+_{VSL} \left[= \left(\frac{f_F}{2} \right)^{0.5} \frac{\rho_l u \delta_{VSL}}{\mu_l} \right]$, for the turbulent heat transfer in a short vertical tube under velocities controlled are clarified based on the numerical solutions.

It was confirmed in this study that authors' steady-state turbulent heat transfer correlation, Eq. (1), based on the experimental data [1]

$$Nu_{d} = 0.02 Re_{d}^{0.85} Pr^{0.4} \left(\frac{L}{d}\right)^{-0.08} \left(\frac{\mu_{l}}{\mu_{w}}\right)^{0.14}$$
 (1)

can not only describe the experimental data of steady-state turbulent heat transfer but also the numerical solutions within ± 10 % difference for the wide ranges of temperature differences between heater inner surface temperature and liquid bulk mean temperature (ΔT_L =5 to 200 K) and flow velocity (u=4.01 to 41.07 m/s).

Keywords

Computational Study, Turbulent Heat Transfer, Heating of Water, Short Vertical Tube, Velocities Controlled

1. Introduction

Computational study of turbulent heat transfer for heating of water in a short vertical tube is important as a detailed knowledge of turbulent heat transfer in pipes and a database for the design of a diverter in a nuclear fusion facility. However, there have been little fundamental work for heating of water and little is known about the effects of heated length, L, on local surface temperature, $(T_s)_z$, local average liquid temperature, $(T_{f,av})_z$, and local liquid pressure drop, ΔP_z .

Many researchers have experimentally studied the steady-state turbulent heat transfer in pipes and given the correlations for calculating steady-state turbulent heat transfer coefficients [2-6].

•Dittus and Boelter:
$$Nu_d = 0.023 Re_d^{0.8} Pr^{0.4}$$
 (2)

• Nusselt:
$$Nu_d = 0.036 Re_d^{0.8} Pr^{1/3} \left(\frac{d}{L}\right)^{0.055}$$
 (3)

• Sieder and Tate:
$$Nu_d = 0.027 Re_d^{0.8} Pr^{1/3} \left(\frac{\mu}{\mu_w}\right)^{0.14}$$
 (4)

•Petukhov:
$$Nu_d = \frac{(f/2)Re_d Pr}{1.07 + 12.7(f/2)^{1/2}(Pr^{2/3} - 1)}$$
 (5)

$$f = (3.64 \log_{10} Re_d - 3.28)^{-2} \tag{6}$$

•Gnielinski:
$$Nu_d = \frac{(f/2)(Re_d - 1000)Pr}{1 + 12.7(f/2)^{1/2}(Pr^{2/3} - 1)}$$
 (7)

All properties in these equations are evaluated at the average bulk liquid temperature, $T_L = (T_{in} + T_{out})/2$, except μ_w , which is evaluated at the wall temperature.

Quite recently, the authors have systematically measured the twisted-tape-induced swirl flow heat transfer due to exponentially increasing heat inputs with various exponential periods $(Q=Q_0exp(t/\tau), \tau=7, 14 \text{ and } 23 \text{ s})$ and the twisted-tape-induced pressure drop with mass velocities, G, ranging from 4022 to 15140 kg/m²s by an experimental water loop flow. Measurements were made on a 59.2 mm effective length which was spot-welded two potential taps on the outer surface of Platinum circular test tube of a 6 mm inner diameter, a 69.6 mm heated length and a 0.4 mm thickness. The twisted tapes with twist ratios, $y = H/d = (pitch of 180^{\circ})$ rotation)/d], of 2.39, 3.39 and 4.45 were used. The relation between the swirl velocity and the pump input frequency and that between the fanning friction factor (f_F) and Reynolds number $(Re_d=2.04\times10^4 \text{ to } 9.96\times10^4)$ were clarified. The twisted-tape-induced swirl flow heat transfers with y=2.39, 3.39 and 4.45 were compared with the values calculated by authors' correlation of the steady-state turbulent heat transfer for the empty tube and other worker's one for the circular tube with the twisted-tape insert. The influence of y and Reynolds numbers based on swirl velocity, Re_{sw}, on the twisted-tape-induced swirl flow heat transfer was investigated into details, and the widely and precisely predictable correlations of the twisted-tape-induced swirl flow heat transfer were derived based on the experimental data [7, 8].

$$Nu_{d} = 0.02 \, Re_{sw}^{0.85} \, Pr^{0.4} \left(\frac{L}{d}\right)^{-0.08} \left(\frac{\mu_{l}}{\mu_{w}}\right)^{0.14} \tag{8}$$

$$Re_{sw} = \frac{\rho_l u_{sw} d}{\mu_l} = Re_d \frac{\pi d^2}{\pi d^2 - 4w\delta_T} \times \frac{(4y^2 + 2\pi^2)^{0.5}}{2y}$$
(9)

The correlations can describe the twisted-tape-induced swirl flow heat transfer for the wide ranges of twist ratios (y=2.39 to 4.45), mass velocities (G=4022 to 15140 kg/m²s) and Reynolds numbers based on swirl velocity (Re_{sw} =2.88×10⁴ to 1.22×10⁵) within -10 to +30 % difference.

The present work has the following objectives: (1) to measure the steady-state turbulent heat transfer coefficients on Platinum test tube divided into three sections (upper, mid and lower positions) for the wide ranges of test tube surface temperature (T_s) and flow velocity (u), (2) to obtain the numerical solutions of surface heat flux, q, and surface temperature, T_s , on the heated length, and liquid temperature, T_f , liquid pressure, P, and flow velocity, u, in the 6-mm inner diameter from theoretical equations for turbulent heat transfer under the same condition as the experimental one, (3) to compare above results with experimental data of surface heat flux, q, local surface temperature, $(T_s)_z$, local average liquid temperature, $(T_{f,av})_z$, and local liquid pressure drop, ΔP_z , (4) to confirm the validity for the component equations in the turbulent heat transfer correlation in a short vertical tube such as liquid temperatures and pressures from inlet to outlet (5) to clarify the thickness of viscous sub-layer, $\delta_{VSL}[=(\Delta r)_{out}/2]$, and the non-dimensional thickness of viscous sub-layer, $y^+_{VSL}[=(f_F/2)^{0.5}\rho_l u \delta_{VSL}/\mu_l]$, for the turbulent heat transfer in a short vertical tube under velocities controlled, where f_F is fanning friction factor, and (6) to discuss the influence of the thickness of viscous sub-layer, δ_{VSL} , and the non-dimensional thickness of viscous sub-layer, y^+_{VSL} , on turbulent heat transfer in a short vertical tube under velocities controlled.

2. Experimental apparatus and method

2.1 Experimental water loop

The schematic diagram of experimental water loop comprised of the pressurizer is shown in Fig. 1. The loop is made of SUS304 stainless steel and is capable of working up to 2 MPa. The loop has five test sections whose inner diameters are 2, 3, 6, 9 and 12 mm. Test sections were vertically oriented with water flowing upward. The test section of the inner diameter of 6 mm was used in this work. The circulating water was distilled and deionized with about 0.2-uS/cm specific resistivity. The circulating water through the loop was heated or cooled to keep a desired inlet temperature by pre-heater or cooler. The flow velocity was measured by a mass flow meter using a vibration tube (Nitto Seiko, CLEANFLOW 63FS25, Flow range=100 and 750 kg/min). The mass velocity was controlled by regulating the frequency of the three-phase alternating power source to the canned type circulation pump (Nikkiso Co., Ltd., Non-Seal Pump Multistage Type VNH12-C4 C-3S7SP, pump flow rate=12 m³/h, pump head=250 m) with an inverter installed a 4-digit LED monitor (Mitsubishi Electric Corp., Inverter, Model-F720-30K). The pump input frequency shows the net pump input power and pump discharge pressure free of slip loss. The water was pressurized by saturated vapor in the pressurizer in this work. The pressure at the outlet of the test tube was controlled within ± 1 kPa of a desired value by using a heater controller of the pressurizer.

2.2 Test section

The cross-sectional view of 6-mm inner diameter test section used in this work is shown in Fig. 2. The Platinum (Pt) test tube for the test tube inner diameter, d, of 6 mm, the heated length, L, of

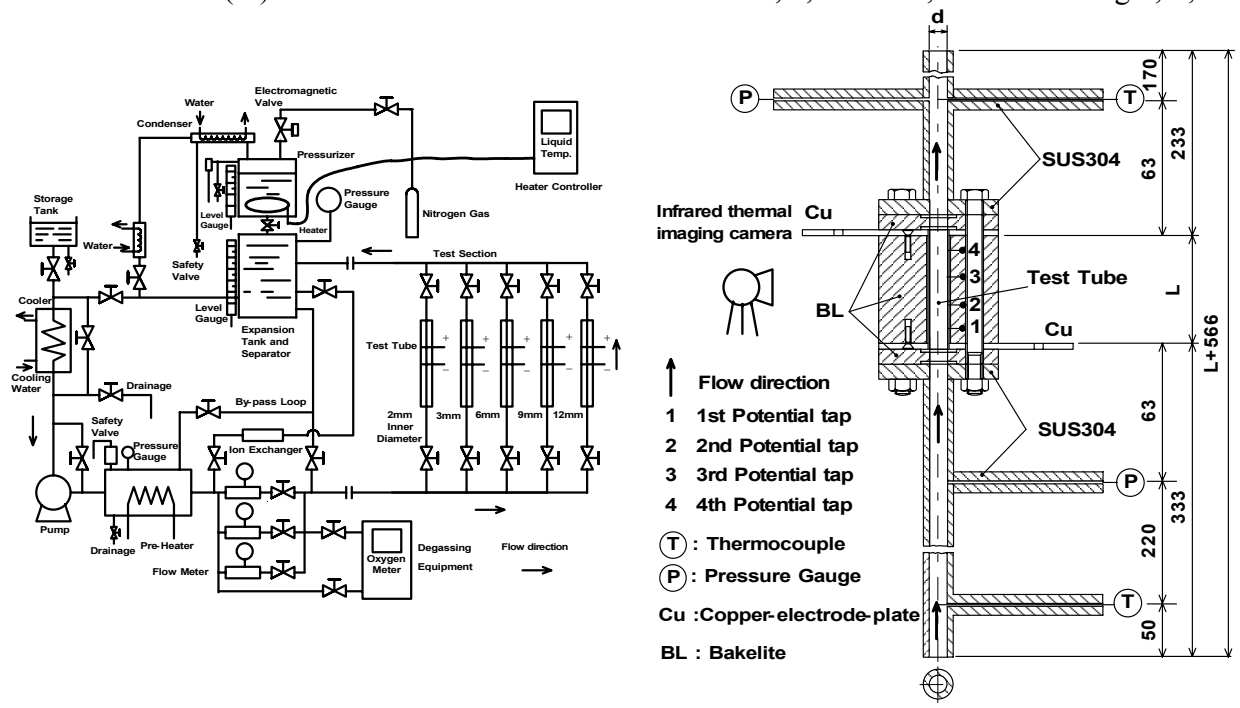


Fig. 1 Schematic diagram of experimental water loop

Fig. 2 Vertical cross-sectional view of 6-mm inner diameter test section

69.6 mm with the commercial finish of inner surface was mainly used in this work. The Platinum test tube is highly sensitive for a resistance thermometry. Wall thickness of the test tube, δ , was 0.4 mm. Four fine 0.07-mm diameter platinum wires were spot-welded on the outer surface of the test tube as potential taps: the first one is at the position of 5.2 mm from the leading edge of the test tube, and the second to forth ones are at 19.6, 20.0 and 19.6 mm from the previous ones, respectively. The effective length, L_{eff} , of the test tube between the first potential tap and forth one on which heat transfer was measured was 59.2 mm. The silver-coated 5-mm thickness copper-electrode-plates to supply heating current were soldered to the surfaces of the both ends of the test tube. The both ends of test tube were electrically isolated from the loop by Bakelite plates of 14-mm thickness. The inner surface condition of the test tube was observed by the scanning electron microscope (SEM) photograph (JEOL JXA8600) and inner surface roughness was measured by Tokyo Seimitsu Co., Ltd.'s surface texture measuring instrument (SURFCOM 120A). Figure 3 shows the SEM photograph of the Platinum (Pt) test tube for d=6 mm with commercial finish of inner surface. The values of inner surface roughness for Ra, Rmax and Rz were measured 0.45, 2.93 and 1.93 µm, respectively.

2.3 Method of heating test tube

The Pt test tube has been heated with an exponentially increasing heat input supplied from a direct current source (Takasago Ltd., NL035-500R, DC 35 V-3000 A) through the two copper electrodes shown in Fig. 4. Heat transfer processes caused by exponentially increasing heat inputs, $Q_0 \exp(t/\tau)$, were measured for the Pt test tube. The exponential periods, τ , of the heat input ranged from 6.04 to 23.66 s. The common specifications of the direct current source are as follows. Constant-voltage (CV) mode regulation is a 4.75 mV minimum, CV mode ripple is 500 μ V r.m.s. or better and CV mode transient response time is less than 200 μ sec (Typical) against

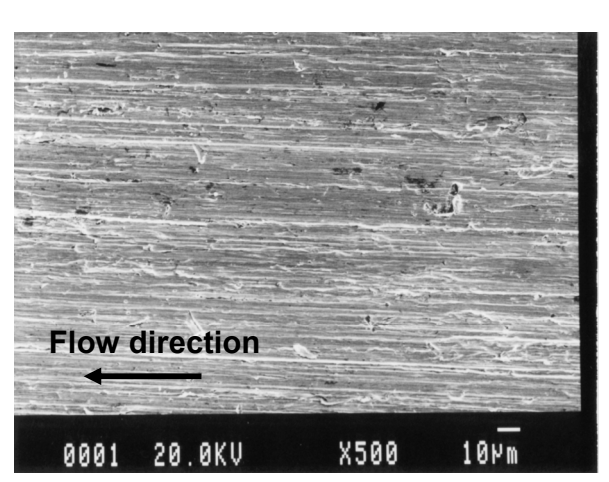


Fig. 3 SEM photograph of the Platinum test tube for an inner diameter of 6 mm with commercial finish of inner surface

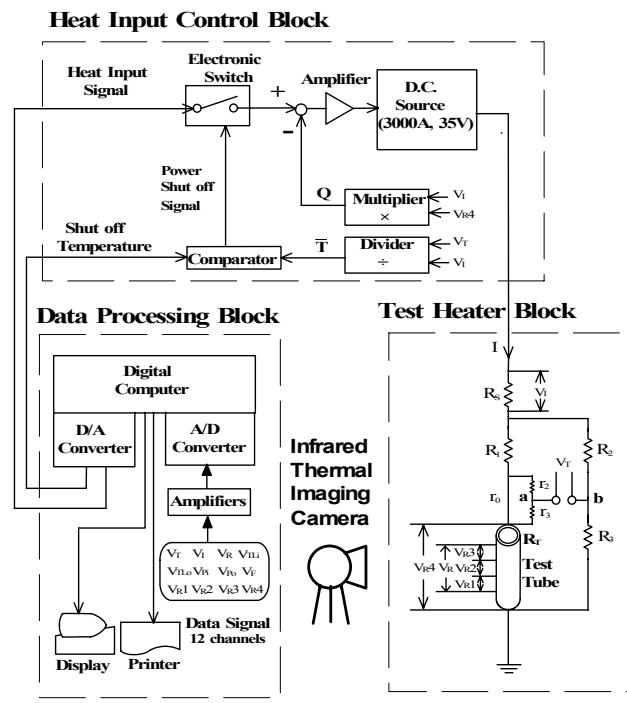


Fig. 4 Measurement and data processing system

5 % to full range change of load.

The outer surface temperature of the test tube with heating was observed by an infrared thermal imaging camera (NEC Avio Infrared Technologies Co., Ltd. Thermography TVS-200EX). The accuracy is ± 2 % of reading. The outer surface of the test tube was uniformly painted black with black body spray (Japan Sensor Corporation, JSC-3, emissivity, ε , of 0.94) in this work.

2.4 Measurement of heat flux, temperature and pressure for test tube

The average temperature of the Pt test tube was measured with resistance thermometry participating as a branch of a double bridge circuit for the temperature measurement. The output voltages from the bridge circuit together with the voltage drop across the potential taps of the test tube (first and forth potential taps, first and second ones, second and third ones, and third and fourth ones) and across a standard resistance were amplified and then were sent via a D/A converter to a digital computer. These voltages were simultaneously sampled at a constant interval ranging from 60 to 200 ms. The average temperatures of the Pt test tube between the first and forth potential taps and between adjacent potential taps (first and second potential taps, second and third ones, and third and forth ones) were calculated with the aid of previously calibrated resistance-temperature relation, respectively. The average temperatures of the test tube between the two electrodes were compared with those between first and fourth potential taps and much difference for a heat loss could not be clearly observed in high subcooling range. The heat generation rates of the Pt test tube between the first and forth potential taps and between adjacent potential taps (first and second potential taps, second and third ones, and third and forth ones) were calculated from the measured voltage difference between the first and forth potential taps and between adjacent potential taps of the Pt test tube, and that across the standard resistance. The surface heat fluxes between the first and forth potential taps and between adjacent potential taps are the differences between the heat generation rate per unit surface area and the rate of change of energy storage in the Pt test tube obtained from the faired average temperature versus time curve as follows:

$$q(t) = \frac{V}{S} \left(Q(t) - \rho c \frac{d\overline{T}}{dt} \right) \tag{10}$$

where ρ , c, V and S are the density, the specific heat, the volume and the inner surface area of the Pt test tube, respectively.

The heater inner surface temperatures between the first and forth potential taps and between adjacent potential taps were also obtained by solving the steady one-dimensional heat conduction equation in the test tube under the conditions of measured average temperature and surface heat flux of the test tube. The solutions for the inner and outer surface temperatures of the test tube, T_s and T_{so} , are given by the steady one-dimensional heat conduction equation. The basic equation for the test tube is as follows:

$$\frac{d^2T}{dr^2} + \frac{1}{r}\frac{dT}{dr} + \frac{Q}{\lambda} = 0 \tag{11}$$

then integration yields and the mean temperature of the test tube is obtained.

$$T(r) = -\frac{Qr^2}{4\lambda} + \frac{Qr_o^2}{2\lambda} \ln r + C \tag{12}$$

$$\overline{T} = \frac{1}{\pi (r_o^2 - r_i^2)} \int_{r_i}^{r_o} 2\pi r T(r) dr \tag{13}$$

Generating heat in the tube is equal to the heat conduction and the test tube is perfectly insulated.

$$q = -\lambda \frac{dT}{dr}\Big|_{r=r_i} = \frac{\left(r_o^2 - r_i^2\right)Q}{2r_i} \tag{14}$$

$$\left. \frac{dT}{dr} \right|_{r=r_0} = 0 \tag{15}$$

The temperatures of the heater inner and outer surfaces, T_s and T_{so} , and C in Eq. (12) can be described as follows:

$$T_{s} = T(r_{i}) = \overline{T} - \frac{qr_{i}}{4(r_{o}^{2} - r_{i}^{2})^{2} \lambda} \times \left[4r_{o}^{2} \left\{ r_{o}^{2} \left(\ln r_{o} - \frac{1}{2} \right) - r_{i}^{2} \left(\ln r_{i} - \frac{1}{2} \right) \right\} - \left(r_{o}^{4} - r_{i}^{4} \right) \right] - \frac{qr_{i}}{2(r_{o}^{2} - r_{i}^{2}) \lambda} \left(r_{i}^{2} - 2r_{o}^{2} \ln r_{i} \right)$$
 (16)

$$T_{so} = T(r_o) = \overline{T} - \frac{qr_i}{4(r_o^2 - r_i^2)^2 \lambda} \times \left[4r_o^2 \left\{ r_o^2 \left(\ln r_o - \frac{1}{2} \right) - r_i^2 \left(\ln r_i - \frac{1}{2} \right) \right\} - \left(r_o^4 - r_i^4 \right) \right] - \frac{qr_i r_o^2}{2(r_o^2 - r_i^2) \lambda} \left(1 - 2 \ln r_o \right)$$
 (17)

$$C = \overline{T} - \frac{qr_i}{4(r_o^2 - r_i^2)^2 \lambda} \times \left[4r_o^2 \left\{ r_o^2 \left(\ln r_o - \frac{1}{2} \right) - r_i^2 \left(\ln r_i - \frac{1}{2} \right) \right\} - \left(r_o^4 - r_i^4 \right) \right]$$
(18)

In case of the 6-mm inner diameter test section, before entering the test tube, the test water flows through the tube with the same inner diameter of the Pt test tube to form the fully developed velocity profile. The entrance tube length, L_e , is given 333 mm ($L_e/d=55.5$). The value of L_e/d for d=6 mm in which the center line velocity reaches 99 % of the maximum value for turbulence flow was obtained ranging from 9.8 to 21.9 by the correlation of Brodkey and Hershey [9] as follows:

$$\frac{L_e}{d} = 0.693 \, Re_d^{1/4} \tag{19}$$

The inlet and outlet liquid temperatures were measured by 1-mm o.d., sheathed, K-type thermocouples (*Nimblox*, sheath material: SUS316, hot junction: ground, response time (63.2 %): 46.5 ms) which are located at the centerline of the tube at the upper and lower stream points of 283 and 63 mm from the tube inlet and outlet points for the 6-mm inner diameter test section. The inlet and outlet pressures were measured by the strain gauge transducers (Kyowa Electronic Instruments Co., Ltd., PHS-20A, Natural frequency: approximately 30 kHz), which were located near the entrance of conduit at upper and lower stream points of 63 mm from the tube inlet and outlet points for the *d*=6-mm inner diameter test section. The thermocouples and the transducers were installed in the conduits as shown in Fig. 2.

The inlet and outlet pressures for the 6-mm inner diameter test section were calculated from the pressures measured by inlet and outlet pressure transducers as follows:

$$P_{in} = P_{ipt} - \{ (P_{ipt})_{wnh} - (P_{opt})_{wnh} \} \times \frac{L_{ipt}}{L_{ipt} + L + L_{opt}}$$
 (20)

$$P_{out} = P_{in} - \left(P_{in} - P_{opt}\right) \times \frac{L}{L + L_{out}} \tag{21}$$

where L_{ipt} =0.063 m and L_{opt} =0.063 m for the 6-mm inner diameter one. Experimental errors are estimated to be ± 1 K in inner tube surface temperature and ± 2 % in heat flux. Mass velocity, inlet and outlet subcoolings, inlet and outlet pressures and exponential period were measured within the accuracy ± 2 %, ± 1 K, ± 4 kPa and ± 2 %, respectively.

3. Numerical solution of turbulent heat transfer

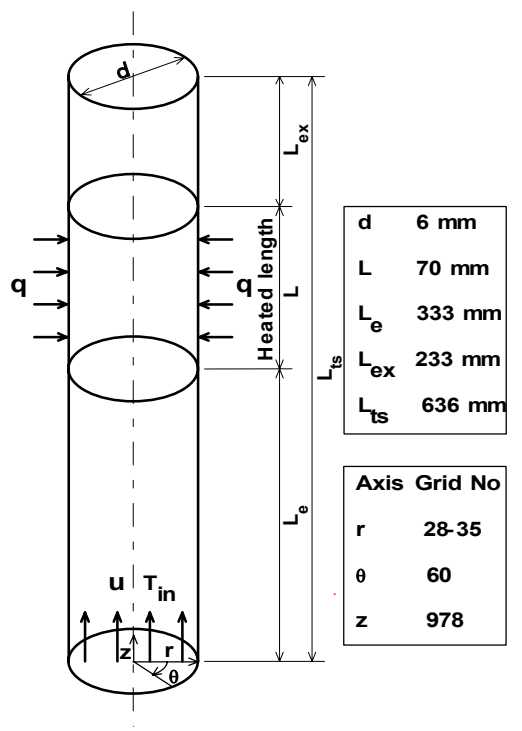


Fig. 5 Physical model for numerical analysis

3.1 Fundamental equations

The unsteady fundamental equations for turbulent heat transfer are expressed in the three dimensional coordinate shown in Fig. 5 as follows [10].

(Continuity Equation)

Cylindrical coordinates (r, θ, z) :

$$\frac{\partial \rho}{\partial t} + \frac{1}{r} \frac{\partial}{\partial r} (\rho r v_r) + \frac{1}{r} \frac{\partial}{\partial \theta} (\rho v_\theta) + \frac{\partial}{\partial z} (\rho v_z) = 0 \tag{22}$$

(Momentum Equation)

r-component:

$$\rho \left(\frac{\partial v_r}{\partial t} + v_r \frac{\partial v_r}{\partial r} + \frac{v_\theta}{r} \frac{\partial v_r}{\partial \theta} - \frac{v_\theta^2}{r} + v_z \frac{\partial v_r}{\partial z} \right) = -\frac{\partial p}{\partial r} - \left(\frac{1}{r} \frac{\partial}{\partial r} (r \tau_{rr}) + \frac{1}{r} \frac{\partial \tau_{r\theta}}{\partial \theta} - \frac{\tau_{\theta\theta}}{r} + \frac{\partial \tau_{rz}}{\partial z} \right) + \rho g_r$$
 (23)

 θ -component:

$$\rho \left(\frac{\partial v_{\theta}}{\partial t} + v_r \frac{\partial v_{\theta}}{\partial r} + \frac{v_{\theta}}{r} \frac{\partial v_{\theta}}{\partial \theta} - \frac{v_r v_{\theta}}{r} + v_z \frac{\partial v_{\theta}}{\partial z} \right) = -\frac{1}{r} \frac{\partial p}{\partial \theta} - \left(\frac{1}{r^2} \frac{\partial}{\partial r} (r^2 \tau_{r\theta}) + \frac{1}{r} \frac{\partial \tau_{\theta\theta}}{\partial \theta} + \frac{\partial \tau_{\thetaz}}{\partial z} \right) + \rho g_{\theta}$$
(24)

z-component:

$$\rho \left(\frac{\partial v_z}{\partial t} + v_r \frac{\partial v_z}{\partial r} + \frac{v_\theta}{r} \frac{\partial v_z}{\partial \theta} + v_z \frac{\partial v_z}{\partial z} \right) = -\frac{\partial p}{\partial z} - \left(\frac{1}{r} \frac{\partial}{\partial r} (r \tau_{rz}) + \frac{1}{r} \frac{\partial \tau_{\theta z}}{\partial \theta} + \frac{\partial \tau_{zz}}{\partial z} \right) + \rho g_z$$
 (25)

(Energy Equation)

Cylindrical coordinates (r, θ, z) :

$$\rho c_{v} \left(\frac{\partial T}{\partial t} + v_{r} \frac{\partial T}{\partial r} + \frac{v_{\theta}}{r} \frac{\partial T}{\partial \theta} + v_{z} \frac{\partial T}{\partial z} \right) = - \left[\frac{1}{r} \frac{\partial}{\partial r} (rq_{r}) + \frac{1}{r} \frac{\partial q_{\theta}}{\partial \theta} + \frac{\partial q_{z}}{\partial z} \right]$$
(26)

where

$$\tau_{rr} = -\mu \left[2 \frac{\partial v_r}{\partial r} - \frac{2}{3} (\nabla \cdot v) \right]$$
 (27),
$$\tau_{\theta\theta} = -\mu \left[2 \left(\frac{1}{r} \frac{\partial v_{\theta}}{\partial \theta} + \frac{v_r}{r} \right) - \frac{2}{3} (\nabla \cdot v) \right]$$
 (28)

$$\tau_{zz} = -\mu \left[2 \frac{\partial v_z}{\partial z} - \frac{2}{3} (\nabla \cdot v) \right]$$
 (29),
$$\tau_{r\theta} = \tau_{\theta r} = -\mu \left[r \frac{\partial}{\partial r} \left(\frac{v_{\theta}}{r} \right) + \frac{1}{r} \frac{\partial v_r}{\partial \theta} \right]$$
 (30)

$$\tau_{\theta z} = \tau_{z\theta} = -\mu \left[\frac{\partial v_{\theta}}{\partial z} + \frac{1}{r} \frac{\partial v_{z}}{\partial \theta} \right]$$
 (31),
$$\tau_{zr} = \tau_{rz} = -\mu \left[\frac{\partial v_{z}}{\partial r} + \frac{\partial v_{r}}{\partial z} \right]$$

$$(\nabla \cdot v) = \frac{\partial v_r}{\partial r} + \frac{1}{r} \frac{\partial v_\theta}{\partial \theta} + \frac{\partial v_z}{\partial z}$$
 (33)

 v_r , v_θ and v_z are the r, θ and z components of a velocity vector, respectively.

3.2 Boundary conditions

The fundamental equations are numerically analyzed together with the following boundary conditions. On the outer boundary of heated section: constant heat flux, and non-slip condition.

$$q = -\lambda \frac{\partial T}{\partial r} = constant \tag{34}$$

At the outer boundary of non-heated section:

$$\frac{\partial T}{\partial r} = 0 \tag{35}$$

At the lower boundary:

$$T = T_{in}$$
, $v_r = 0$, $v_{\theta} = 0$ and $v_z = u$ for in-flow,

where T_{in} and u are a inlet liquid temperature and a flow velocity at the entrance of the test section.

3.3 Method of solution

The control volume discretization equations were derived from these fundamental equations by using the hybrid scheme [11]. The thermo-physical properties for each control volume are given

as those at each volume temperature. The procedure for the calculation of the flow field is the SIMPLE algorithm which stands for Semi-Implicit Method for Pressure-Linked Equations.

The surface heat fluxes, q, for the heated length were equally given in the range of 2.55×10^5 to 3.63×10^7 W/m² as an initial condition, and numerical calculation was continued until the steady-state was obtained. The surface temperature on the test tube, T_s , was calculated from the analyzed temperature of the outer control volume on the test tube surface, TEM, which is supposed to be located on the center of the control volume, by solving the heat conduction equation in liquid, $T_s = (\Delta r)_{out} q/2\lambda_l + TEM$. Average heat transfer coefficient on the test tube surface was obtained by averaging the calculated local surface temperatures at every 0.5 mm in the heated length, L. All the calculations were made by using the PHOENICS code [12].

4. Experimental results and discussion

4.1 Experimental conditions

Steady-state heat transfer processes on the Pt test tube that caused by the exponentially increasing heat inputs, $Q_0 exp(t/\tau)$, were measured. The exponential periods, τ , of the heat input ranged from 6.04 to 23.66 s. The initial experimental conditions such as inlet flow velocity, inlet liquid temperature, inlet pressure and exponential period for the single-phase flow heat transfer experiment were determined independently each other before each experimental run.

The experimental conditions were as follows:

Heater material Surface condition Commercial finish of inner surface Surface roughness for Ra, Rmax and Rz 0.45, 2.93 and 1.93 μm Inner diameter (*d*) 6 mm Heated length (L)69.6 mm Effective Length (L_{eff}) 59.2 mm L_{12} 19.6mm, L_{23} $20.0 \text{ mm}, L_{34}$ 19.6 mm L/d11.6 L_{eff}/d 9.87 Wall thickness (δ) 0.4 mm Inlet flow velocity (*u*) 4.11, 7.12, 10.07, 13.62, 21.43, 30.72 and 41.07 m/s Inlet pressure (P_{in}) 810.40 to 1044.21 kPa Outlet pressure (P_{out}) 795.47 to 846.33 kPa Inlet subcooling ($\Delta T_{sub,in}$) 142.82 to 147.47 K Outlet subcooling ($\Delta T_{sub.out}$) 136.26 to 141.09 K 296.47 to 310.04 K Inlet liquid temperature (T_{in}) Exponentially increasing heat input (*Q*) $Q_0 \exp(t/\tau)$, $\tau = 6.04$ to 23.66 s

4.2 Parameters for calculation

The parameters used for calculation were as follows:

Inner diameter (<i>d</i>)	6 mm
Heated length (L)	70 mm
Entrance length (L_e)	333 mm
Exit length (L_{ex})	33 mm
Test section length (L_{ts})	636 mm
Heat flux (q)	2.55×10^5 to 3.63×10^7 W/m ² ($q_0 \exp(t/\tau)$, $\tau = 21.80$ to 22.53 s)
Inlet flow velocity (<i>u</i>)	4.11, 7.12, 10.07, 13.62, 21.43, 30.72 and 41.07 m/s
Inlet liquid temperature (T_{in})	296.47 to 310.04 K
Coordinate system	cylindrical coordinate (r, θ, z)
Grid number	(28 to 35, 60, 978)
Physical model	high Reynolds number form of k-epsilon model

4.3 Inlet and outlet pressures, P_{in} and P_{out} , and pressures measured by the inlet and outlet pressure transducers, P_{ipt} and P_{opt}

Figure 6 shows the z-axis variations of the pressures measured by the inlet and outlet pressure transducers, P_{ipt} and P_{opt} , and the inlet and outlet pressures calculated by Eqs. (20) and (21), P_{in} and P_{out} , for the inlet liquid temperature, T_{in} , of 302.68 K and the flow velocity, u, of 13.51 m/s at the fanning friction factor, f_F , of 0.008. The value of P_{ipt} at the distance from inlet of the test section, Z=0.27 m, kept almost constant in the whole experimental range as they are controlled within ± 1 kPa of the desired value by using a heater controller of the pressurizer, and then the value of P_{opt} at Z=0.466 m became considerably lower. The values of P_{in} and P_{out} were obtained 844.63 and 807.06 kPa from 877.50 and 773.05 kPa of P_{ipt} and P_{opt} at the elapsed time of 127.2 s by Eqs. (20) and (21), respectively and then the local liquid pressure drop, ΔP_z , between the heated length, L, of the test section is almost 37.57 kPa. The numerical solutions of liquid pressure, P, on the test section are also shown as red solid line in the figure for comparison. The pressure of 233.28 kPa at the entrance of the test section, Z=0 m, become LINEARLY smaller with an increase in the z-axis distance, Z, and almost constant about 0 kPa at the exit of the test section, Z=0.636 m, although the pressure drop of these solutions between the heated length (ΔP_z =23.46 kPa) became 37.6 % lower than that of the experimental data (ΔP_z =37.57 kPa).

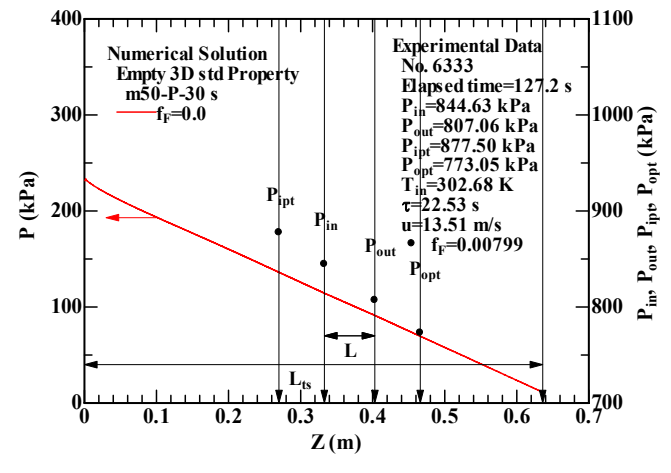


Fig. 6 Z-axis distributions of pressures measured, P_{ipt} and P_{opt} , and those calculated, P_{in} and P_{out} , for T_{in} =302.68 K, u=13.51 m/s and f_{ir} =0.008 compared with numerical solutions of liquid pressure, P

There would be various reasons as follows. For one reason, the inner surface roughness of the Pt test tube for d=6 mm with commercial finish of inner surface was measured by Tokyo Seimitsu Co., Ltd.'s surface texture measuring instrument (SURFCOM 120A). The values of inner surface roughness for Ra, Rmax and Rz were measured 0.45, 2.93 and 1.93 μ m, respectively. However, the default value of the roughness height in the PHOENICS code was given 0.0, which defines a hydro-dynamically smooth wall. It would be true from this fact that the authors have derived Eqs. (20) and (21) by the use of linear interpretation for the calculation of inlet and outlet pressures, P_{in} and P_{out} , from non-boiling heat transfer to CHF point through nucleate boiling heat transfer, although the numerical solutions would have some errors due to the difference of experimental and computational conditions and these pressures, P_{ipt} and P_{opt} , have been measured at high Jakob number in this work, not under liquid-vapor two-phase flow.

4.4 Inner and outer surface temperatures, T_s and T_{so} , heat fluxes, q, and heat transfer coefficients, h, for 1st, 2nd and 3rd positions of three sections, and inlet and outlet liquid temperatures, T_{in} and T_{out}

Figures 7 and 8 show inner surface temperatures (T_{s1} , T_{s2} and T_{s3} -black solid circles), outer surface temperatures (T_{sol} , T_{so2} and T_{so3} -black open circles), heat fluxes (q_1 , q_2 and q_3 -black solid triangles) and heat transfer coefficients (h_1 , h_2 and h_3 - black open triangles) for first, second and third positions of the sections between first and second potential taps, second and third ones and third and fourth ones, and inlet and outlet liquid temperatures (T_{in} and T_{out} -black solid squares) at the flow velocities, u, of 13.59 and 30.72 m/s with the heat fluxes, q, of 8.44 and 8.84 MW/m², respectively. The liquid temperatures at the center of each section (heated lengths, L, of 15, 34.8 and 54.6 mm-black open squares) are linearly estimated from the values of the inlet liquid temperature, T_{in} , and outlet one, T_{out} . The inner surface temperatures (T_{sol} , T_{sol} and T_{sol}) were obtained from Eqs. (16) and (17) with the measured average temperature and surface heat flux. The inner and outer surface temperatures

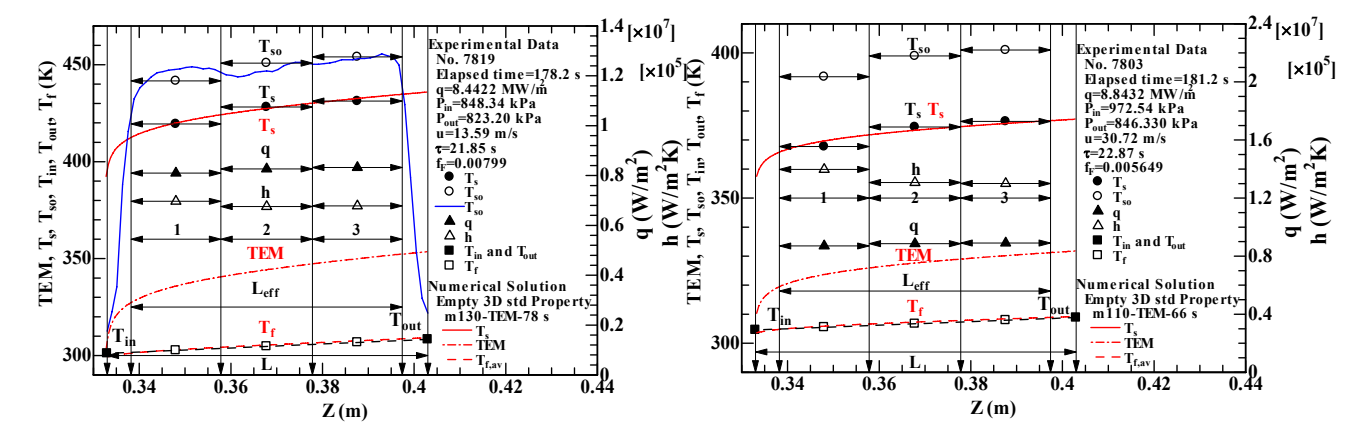


Fig. 7 Inner and outer surface temperatures, heat fluxes and heat transfer coefficients for first, second and third positions of three sections, and inlet and outlet liquid temperatures for the exponential period of 21.85 s at the flow velocity of 13.59 m/s compared with numerical solutions of inner surface temperature and outer surface temperature observed by an infrared thermal imaging camera

Fig. 8 Inner and outer surface temperatures, heat fluxes and heat transfer coefficients for first, second and third positions of three sections, and inlet and outlet liquid temperatures for the exponential period of 22.87 s at the flow velocity of 30.72 m/s compared with numerical solutions of inner surface temperature

Log Number: 173

for each position of the sections (T_{s1} , T_{s2} and T_{s3} , and T_{so1} , T_{so2} and T_{so3}) become gradually higher with an increase in the heated length from the leading edge of the test tube, whereas the heat fluxes (q_1 , q_2 and q_3) are almost constant for each position of the sections. The increasing rate of the inner surface temperature shows nearly the same trend of that of the liquid temperature from the inlet to the outlet (T_{in} to T_{out}). The heat transfer coefficients for each position of the sections (h_1 , h_2 and h_3) become almost constant as shown in the figure.

The numerical solutions of the z-axis variations in the analyzed liquid temperature of the outer control volume on the test tube surface, TEM, are shown at the heat fluxes of 8.49 and 8.84 MW/m² with the flow velocities of 13.59 and 30.72 m/s as a red 1-dot dashed line. The surface temperatures on the test tube, T_s , were calculated from the analyzed liquid temperature of the outer control volume on the test tube surface, TEM, which is supposed to be located on the center of the control volume, by solving the heat conduction equation in liquid, $T_s = (\Delta r)_{out} q/2\lambda_l + TEM$. The z-axis variations in the inner surface temperature of the test tube at every 0.5 mm in the heated length, L, are shown as red solid line in the figure. They become gradually higher with an increase in the z-axis distance from the leading edge of the test tube. The numerical solutions of the inner surface temperatures solved by the theoretical equations for turbulent heat transfer, Eqs. (22) to (35), are in good agreement with the experimental data given by Eq. (16) which are obtained from the steady one-dimensional heat conduction equation.

The outer surface temperature of the test tube was observed by an infrared thermal imaging camera. The z-axis variations in the outer surface temperature of the test tube, T_{so} , for the exponential period of 21.85 s at the flow velocity of 13.59 m/s with the heat flux of 8.44 MW/m² are shown as a blue solid line in Fig. 7. The outer surface temperature of the test tube steeply increases from 312.54 K at the electrode of the inlet up to 430 K at the heated length of 5 mm from the leading edge of the test tube, and gradually becomes higher, lower and higher again up to the highest value of around 455 K to about 5 mm short of the outlet of the test tube. Finally, it linearly falls down to 322.34 K at the electrode of the outlet again. The both ends of the Platinum test tube were soldered to the copper-electrode-plates which have a width of 80 mm, a length of 120 mm and a thickness of 5 mm. The heat capacities of the copper-electrode-plates with subcooled water flow would be far large in comparison with the joule heat of the test tube which has a wall thickness, δ , of 0.4 mm. The outlet liquid temperature (T_{out} = 310.55 K) becomes 9.46 K higher than the inlet one (T_{in} = 301.09 K) by the uniform heating of the test tube with q=8.44 MW/m². It is observed from this figure that the outer surface temperatures for first, second and third positions of three sections on the blue solid line gradually increase with an increase in the heated length. The increasing rate of the outer surface temperature seems to be the same with that of the liquid temperature from inlet to outlet. It will be considered from this fact that the heat transfer coefficients on the inner surface of the test tube will be almost constant for the heated length in the non-boiling region as mentioned above. The outer surface temperatures with ε =0.94 for first, second and third positions of three sections were 10 to 20 % lower than the values calculated from Eq. (17) derived by Hata and Masuzaki [13], although the infrared thermal imaging camera has the accuracy of ± 2 % of reading. The temperature curves on the figure were uniformly revised to the values calculated from Eq. (17) and plotted.

The numerical solutions of average liquid temperature, $T_{f,av}$, from inlet to outlet are also shown as red broken line in Figs. 7 and 8 for comparison. The average liquid temperatures, $T_{f,av}$, were

calculated from the analyzed liquid temperatures of the control volumes on the r and θ -axis grid numbers for each z-axis grid number. Those become linearly higher with an increase in the z-axis distance, Z, and become almost equal to the outlet liquid temperature, T_{out} , at the exit of the heated length. Therefore, it was confirmed from this fact that the heat transfer coefficients, h, calculated from the heat fluxes, q, and the liquid temperatures, T_f , at the heated lengths, L, of 15, 34.8 and 54.6 mm which were obtained by the use of linear interpretation between the inlet and outlet liquid temperatures, T_{in} and T_{out} , would also be true, although these inlet and outlet liquid temperatures were measured by 1-mm o.d., sheathed, K-type thermocouples in the small diameter tube of d=6 mm.

4.5 Steady-state turbulent heat transfer characteristics

Figure 9 shows the typical example of the steady-state turbulent heat transfer curve for Platinum circular tube of d=6 mm and $L_{eff}=59.2$ mm with the exponential period, τ , of around 22.53 s at the flow velocity, u, of 13.51 m/s. The experimental data were compared with the values derived from authors' correlation of the steady-state turbulent heat transfer for the empty tube, Eq. (1), at the flow velocity, u, of 13.51 m/s. The heat fluxes gradually become higher with an increase in the temperature difference between heater inner surface temperature and liquid bulk mean temperature, ΔT_L (= T_s - T_L), on the steady-state turbulent heat transfer curve derived from Eq. (1). These experimental data are compared with the values derived from other workers' correlations of the steady-state turbulent heat transfer in pipes, Eqs. (2) to (7). The experimental data for d=6 mm at the high heat flux point shown in Fig. 9 are 24.7 to 62.7 % higher than the values derived from these correlations at a fixed temperature difference between heater inner surface temperature and average bulk liquid temperature (ΔT_L =constant), and 26 to 75 K lower than the values derived from these correlations at a fixed heat flux (q=constant).

The numerical solutions for the relation between the heat flux, q, and the temperature difference between heater inner surface temperature and average bulk liquid temperature, ΔT_L , are shown

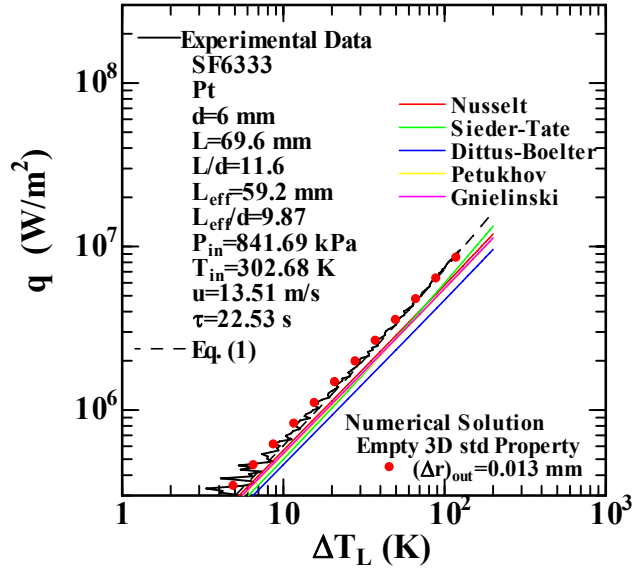


Fig. 9 Relationship between q and ΔT_L [= $(T_s - T_L)$] for circular tube of d=6 mm and L_{eff} =59.2 mm with T_{in} =302.68 K and u=13.51 m/s at P_{in} =841.69 kPa

for the heat flux, q, ranging from 2.55×10^5 to 8.49×10^6 W/m² at the flow velocity of 13.51 m/s as red solid circles. The 12 different values for the numerical solutions are plotted for the heat flux ranging from 3×10^6 to 10^7 on the log-log graph. These solutions become also higher with an increase in the ΔT_L along the curve derived from Eq. (1). The numerical solutions solved by the theoretical equations for turbulent heat transfer, Eqs. (22) to (35), are in good agreement with the experimental data and the values derived from Eq. (1) within ± 10 % difference.

4.6 Radius variations of liquid temperature and flow velocity

Figure 10 shows the radius variations of the liquid temperatures and the flow velocity numerically solved in the tube for the heat flux of 8.49 MW/m² with the heated length, L, varied as a parameter. The flow velocity in the tube becomes parabolically low with a decrease and an increase in the radius from the centerline of the main stream to the outer surface one. The numerical solutions of the liquid temperatures firmly keeps almost the constant value of the inlet liquid temperature, T_{in} , up to the r of around ± 2 mm and those become exponentially and perpendicularly higher with a decrease and an increase in the radius to the inner surface temperatures of the test tube, T_s , at outer surface of the main stream. The viscous sub-layers on the heated length become gradually thicker with an increase in the heated length. The inner surface temperatures, T_s , calculated from the liquid temperature at the outer control volume by the heat conduction equation, $T_s = (\Delta r)_{out} q/2\lambda_l + TEM$, are shown in Fig. 10 as solid circles with each symbol color to clarify the effects of heated length on liquid temperature distribution and thickness of viscous sub-layer on the test tube surface for the steady-state turbulent heat transfer coefficient. The liquid temperatures, T_f , of the main stream for the radius from 0 to ± 2 mm are almost equal to the inlet liquid temperature, T_{in} , along the heated length, L, from 0 mm to 70 mm on the test tube of d=6 mm. For example, the liquid temperature for the heated length, L, of 0.0695 m steeply increases from 353.55 K at the center point of the outer control volume (Δr =13 μm) up to 435.89 K at the outer surface of the control volume, which is the inner surface

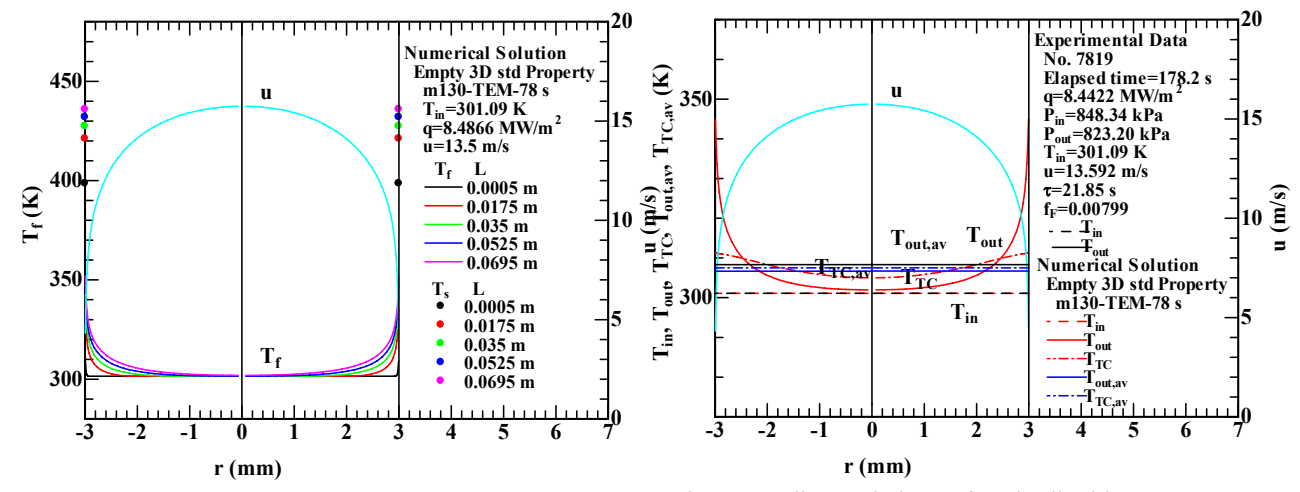


Fig. 10 Radius variation of liquid temperatures and flow velocity numerically solved for heat flux of 8.49 MW/m² at flow velocity of 13.5 m/s

Fig. 11 Radius variations of outlet liquid temperatures, T_{out} and T_{TC} , for numerical solutions compared with outlet liquid temperatures measured in the platinum test tube of d=6 mm with heat flux of 8.44 MW/m² for exponential period of around 21.85 s at flow velocity of 13.59 m/s

temperature, T_s , of the test tube. It is considered especially in case of the high Jacob number that the void fractions would become larger right beneath the test tube surface at the outlet of the test tube, even if the inner surface temperature rapidly jumps from the nucleate boiling heat transfer to the film boiling one at the occurrence of critical heat flux [13-20]. That is, the void fractions on the greater part of the heated length except the outlet of the test tube would become too much smaller such as single phase flow from non-boiling heat transfer to CHF point through nucleate boiling heat transfer.

4.7 Radius variations of outlet liquid temperatures, T_{out} and T_{TC}

The radius variations of outlet liquid temperatures, T_{out} and T_{TC} , for the numerical solutions are shown at the lower stream points of 0.25 mm and 63.015 mm from the test tube outlet point in Fig. 11 as a red solid line and a red 1-dot dashed one, respectively. The liquid temperatures at 0.25 mm from the test tube outlet point, T_{out} , are widely distributed such as those on the heated length, T_f . However, the liquid temperature distribution at 63.015 mm from the test tube outlet point, T_{TC} , that is the point located the outlet thermocouple, become considerably small due to mixing along flow length. The average values of outlet liquid temperatures, T_{out} and T_{TC} , for the numerical solutions are shown as a blue solid line and a blue 1-dot dashed one and those are almost similar to the outlet liquid temperature measured by 1-mm o.d., sheathed, K-type thermocouple, T_{out} , which is shown as a black solid line. It is considered from this fact that the average liquid temperature in a small diameter tube will be precisely measured by one 1-mm o.d., sheathed, K-type thermocouple, although the r-axis variation of the outlet liquid temperature will become considerably large with an increase in heat flux, q.

4.8 Steady-state turbulent heat transfer under u=4.11, 21.43, 30.72 and 41.07 m/s

The steady-state turbulent heat transfer curves for Platinum circular tube of d=6 mm and $L_{eff}=59.2$ mm with the exponential period, τ , of around 22 s under the flow velocities, u, of 4.11,

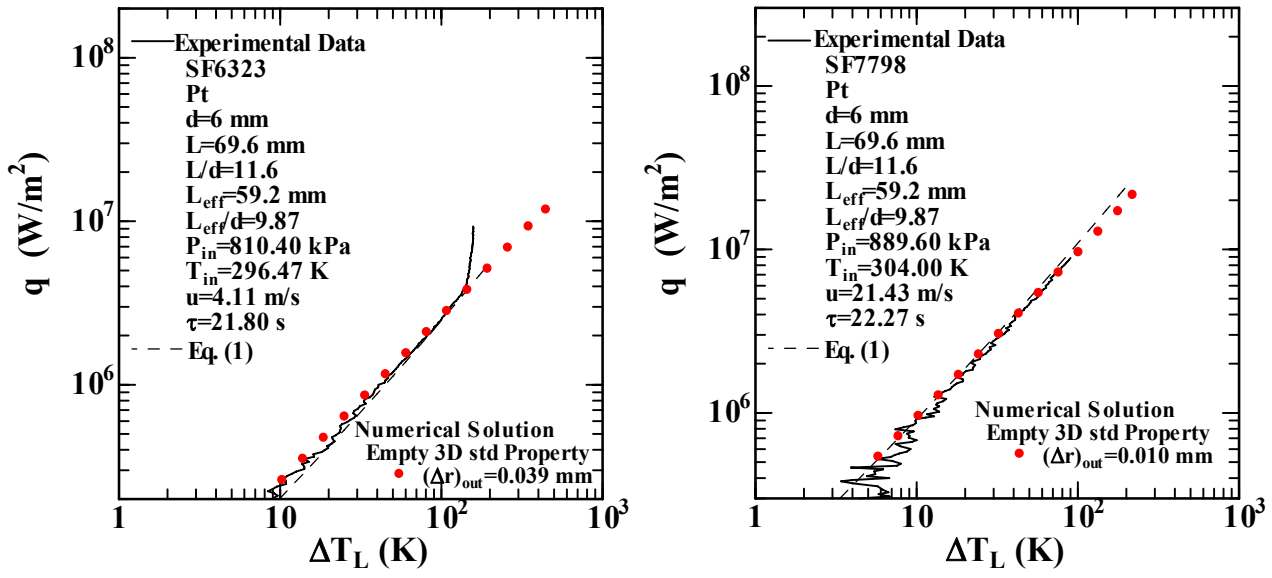


Fig. 12 Relationship between q and ΔT_L [= $(T_s$ - T_L)] for circular tube of d=6 mm and L_{eff} =59.2 mm with T_{in} =296.47 K and u=4.11 m/s at P_{in} =810.40 kPa

Fig. 13 Relationship between q and ΔT_L [= $(T_s$ - T_L)] for circular tube of d=6 mm and L_{eff} =59.2 mm with T_{in} =304.00 K and u=21.43 m/s at P_{in} =889.60 kPa

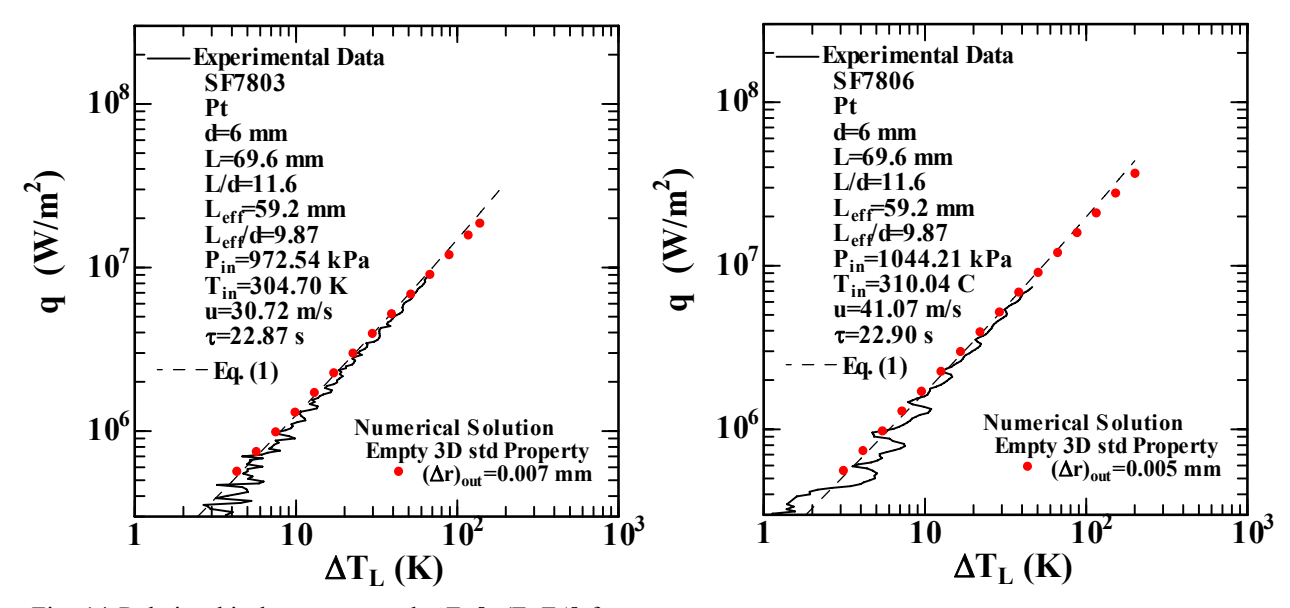


Fig. 14 Relationship between q and ΔT_L [= $(T_s$ - T_L)] for circular tube of d=6 mm and L_{eff} =59.2 mm with T_{in} =304.70 K and u=30.72 m/s at P_{in} =972.54 kPa

Fig. 15 Relationship between q and ΔT_L [= (T_s-T_L)] for circular tube of d=6 mm and L_{eff} =59.2 mm with T_{in} =310.04 K and u=41.07 m/s at P_{in} =1044.21 kPa

21.43, 30.72 and 41.07 m/s are shown in Figs 12 to 15. The experimental data were also compared with the values derived from authors' correlation of the steady-state turbulent heat transfer for the empty tube, Eq. (1), at the flow velocities, u, of 4.11, 21.43, 30.72 and 41.07 m/s. The heat fluxes gradually become higher with an increase in the temperature difference between heater inner surface temperature and liquid bulk mean temperature, ΔT_L (= T_s - T_L), on the steady-state turbulent heat transfer curve derived from Eq. (1).

The numerical solutions for the relation between the heat flux, q, and the temperature difference between heater inner surface temperature and average bulk liquid temperature, ΔT_L , are shown for the heat flux, q, ranging from 2.55×10^5 to 3.63×10^7 W/m² at the flow velocities of 4.11, 21.43, 30.72 and 41.07 m/s as red solid circles, respectively. The 14 to 16 different values for the numerical solutions are plotted for the heat flux ranging from 2.55×10^5 to 3.63×10^7 on the loglog graph. These solutions become also higher with an increase in the ΔT_L along the curve derived from Eq. (1). The numerical solutions solved by the theoretical equations for turbulent heat transfer, Eqs. (22) to (35), are in good agreement with the experimental data and the values derived from Eq. (1) within ± 10 % difference.

4.9 Thickness of viscous sub-layer, δ_{VSL} , and the non-dimensional thickness of viscous sub-layer, y^+_{VSL} , for steady-state turbulent heat transfer

The numerical solutions solved by the theoretical equations for steady-state turbulent heat transfer, Eqs. (22) to (35), are in good agreement with the experimental data and the values derived from Eq. (1) within ± 10 % difference as shown in Figs 9 and 12 to 15. The liquid temperatures on the test tube surface in the viscous sub-layer will become linearly lower with a decrease in the radius by the heat conduction from the surface temperature on the test tube, $T_f = T_s - \Delta r q/\lambda_l$. And let those, T_f , equal the analyzed temperature of the outer control volume on the test tube surface, TEM, in the turbulent flow region, which is supposed to be located on the

center of the control volume, $T_f = T_s - (\Delta r)_{out} \ q/2\lambda_l = TEM$. Half the thickness of the outer control volume, $(\Delta r)_{out}/2$, would become the thickness of the viscous sub-layer, δ_{VSL} , for the turbulent heat transfer in a short vertical tube under velocities controlled. Relationships between δ_{VSL} and the non-dimensional thickness of viscous sub-layer, y^+_{VSL} , for the steady-state turbulent heat transfer numerically solved, and u are shown for the temperature difference between heater inner surface temperature and liquid bulk mean temperature, $\Delta T_L = T_s - T_L$, of 100 K in Fig. 16. Two non-dimensional thicknesses of viscous sub-layer, $(y^+_{VSL})_{TEM}$ and $(y^+_{VSL})_{TL}$, are given as it will be very difficult to solve the analyzed temperature of the outer control volume on the test tube surface, TEM. All properties in the equation are evaluated at the analyzed temperature of the outer control volume on the test tube surface, TEM, and the liquid bulk mean temperature, $T_L = (T_{in} + T_{out})/2$, respectively. The non-dimensional thickness of viscous sub-layer, y^+_{VSL} , is defined as follows:

$$y_{VSL}^{+} = \left(\frac{f_F}{2}\right)^{0.5} \frac{\rho_l u \delta_{VSL}}{\mu_l} \tag{36}$$

where f_F is fanning friction factor. The values of δ_{VSL} become linearly lower with an increase in the flow velocity, u, on the log-log graph, although those of $(y^+_{VSL})_{TEM}$ and $(y^+_{VSL})_{TL}$ become a little higher with an increase in the flow velocity, u, but are almost constant in the whole numerical range. These numerical solutions of δ_{VSL} , $(y^+_{VSL})_{TEM}$ and $(y^+_{VSL})_{TL}$ can be expressed for the u ranging from 4.11 to 41.07 m/s by the following correlations:

$$\delta_{VSL} = 65u^{-0.85}$$
 (37), $(y_{VSL}^+)_{TEM} = 9.08u^{0.1}$ for $\Delta T_L = 100$ K (38), $(y_{VSL}^+)_{TL} = 5.50u^{0.1}$ for $\Delta T_L = 100$ K (39)

These numerical solutions of $(y^+_{VSL})_{TEM}$ and $(y^+_{VSL})_{TL}$ are also shown versus the Reynolds number, Re_d , with the temperature differences between heater inner surface temperature and average bulk liquid temperature, ΔT_L , of 40, 80, 100 and 120 K in Figs. 17 and 18, respectively.

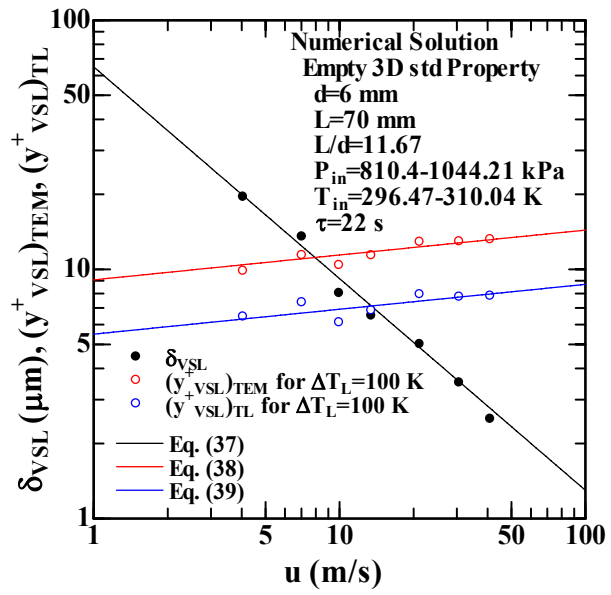


Fig. 16 Relationships between δ_{VSL} , $(y^+_{VSL})_{TEM}$ and $(y^+_{VSL})_{TL}$ for the turbulent heat transfer numerically solved, and u with $\Delta T_L = 100$ K

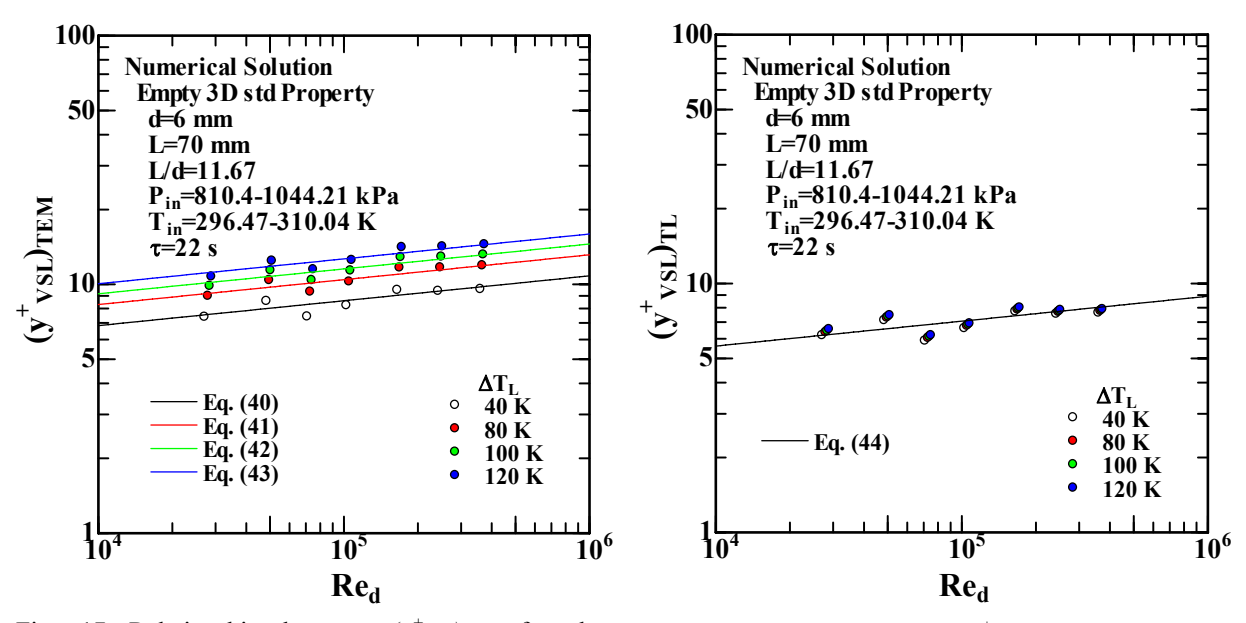


Fig. 17 Relationship between $(y^+_{VSL})_{TEM}$ for the turbulent heat transfer numerically solved, and Re_d with ΔT_L =40, 80, 100 and 120 K

Fig. 18 Relationship between $(y^+_{VSL})_{TL}$ for the turbulent heat transfer numerically solved, and Re_d with ΔT_L =40, 80, 100 and 120 K

These numerical solutions of $(y^+_{VSL})_{TEM}$ and $(y^+_{VSL})_{TL}$ can be expressed for the Re_d ranging from 2.71×10^4 to 3.74×10^5 by the following correlations:

$$(y_{VSL}^{+})_{TEM} = 2.72 Re_d^{-0.1}$$
 for $\Delta T_L = 40 \text{ K}$ (40), $(y_{VSL}^{+})_{TEM} = 3.30 Re_d^{-0.1}$ for $\Delta T_L = 80 \text{ K}$ (41)
 $(y_{VSL}^{+})_{TEM} = 3.65 Re_d^{-0.1}$ for $\Delta T_L = 100 \text{ K}(42)$, $(y_{VSL}^{+})_{TEM} = 4.00 Re_d^{-0.1}$ for $\Delta T_L = 120 \text{ K}(43)$
 $(y_{VSL}^{+})_{TL} = 2.23 Re_d^{-0.1}$ for $\Delta T_L = 40, 80, 100 \text{ and } 120 \text{ K}$ (44)

5. Conclusions

The steady-state turbulent heat transfer coefficients in a short vertical Platinum (Pt) test tube for the flow velocities (u=4.11, 7.12, 10.07, 13.62, 21.43, 30.72 and 41.07 m/s), the inlet liquid temperatures (T_{in} =296.47 to 310.04 K), the inlet pressures (P_{in} =810.40 to 1044.21 kPa) and the increasing heat inputs ($Q_0 exp(t/\tau)$, τ of 6.04 to 23.66 s) were systematically measured. Measurements were made on a 59.2 mm effective length and its three sections (upper, mid and lower positions), which were spot-welded four potential taps on the outer surface of the Pt test tube of a 6 mm inner diameter, a 69.6 mm heated length and a 0.4 mm thickness. Theoretical equations for turbulent heat transfer in a circular tube of a 6 mm in diameter and a 636 mm long were numerically solved for heating of water with heated section of a 6 mm in diameter and a 70 mm long by using PHOENICS code under the same condition as the experimental one considering the temperature dependence of thermo-physical properties concerned. Experimental and computational study results lead to the following conclusions.

- 1) The numerical solution of liquid pressure, P, on the test section becomes 233.28 kPa at the entrance of the test section, Z=0 m. Those become LINEARLY smaller with an increase in the z-axis distance, Z, and almost constant about 0 kPa at the exit of the test section, Z=0.636 m.
- 2) The inner and outer surface temperatures for each position of the three sections (T_{s1} , T_{s2} and T_{s3} , and T_{so1} , T_{so2} and T_{so3}) become gradually higher with an increase in the heated length from

the leading edge of the test tube, whereas the heat fluxes $(q_1, q_2 \text{ and } q_3)$ are almost constant for each position of the sections. The increasing rate of the inner surface temperature shows nearly the same trend of that of the liquid temperature from the inlet to the outlet $(T_{in} \text{ to } T_{out})$. The heat transfer coefficients for each position of the sections $(h_1, h_2 \text{ and } h_3)$ become almost constant.

- 3) The numerical solutions of the inner surface temperatures solved by the theoretical equations for turbulent heat transfer, Eqs. (22) to (35), are in good agreement with the experimental data $(T_{s1}, T_{s2} \text{ and } T_{s3})$ given by Eq. (16) which are obtained from the steady one-dimensional heat conduction equation.
- 4) The numerical solutions for the relation between the heat flux, q, and the temperature difference between heater inner surface temperature and average bulk liquid temperature, ΔT_L , solved by the theoretical equations for turbulent heat transfer, Eqs. (22) to (35), are in good agreement with the experimental data and the values derived from Eq. (1) within ± 10 % difference for the heat flux, q, ranging from 2.55×10^5 to 3.63×10^7 W/m² at the flow velocities of 4.11, 7.12, 10.07, 13.62, 21.43, 30.72 and 41.07 m/s.
- 5) The liquid temperatures, T_f , of the main stream numerically solved for the radius from 0 to ± 2 mm are almost equal to the inlet liquid temperature, T_{in} , along the heated length, L, from 0 mm to 70 mm on the test tube of d=6 mm.
- 6) The average values of outlet liquid temperatures, T_{out} and T_{TC} , for the numerical solutions are almost similar to the outlet liquid temperature measured by one 1-mm o.d., sheathed, K-type thermocouple, T_{out} .
- 7) The thickness of the viscous sub-layer, δ_{VSL} , which is half the thickness of the outer control volume, $(\Delta r)_{out}/2$, become linearly lower with an increase in the flow velocity, u, on the loglog graph, although the values of the non-dimensional thickness of viscous sub-layer, $(y^+_{VSL})_{TEM}$ and $(y^+_{VSL})_{TL}$, become a little higher with an increase in the flow velocity, u, but are almost constant in the whole numerical range. These numerical solutions of δ_{VSL} , $(y^+_{VSL})_{TEM}$ and $(y^+_{VSL})_{TL}$ can be expressed for the u ranging from 4.11 to 41.07 m/s by the following correlations:

$$\delta_{VSL} = 65u^{-0.85} \quad (37), \quad (y_{VSL}^{+})_{TEM} = 9.08u^{0.1} \quad \text{for } \Delta T_{L} = 100 \text{ K} \quad (38), \quad (y_{VSL}^{+})_{TL} = 5.50u^{0.1} \quad \text{for } \Delta T_{L} = 100 \text{ K} \quad (39)$$

$$(y_{VSL}^{+})_{TEM} = 2.72 Re_{d}^{0.1} \quad \text{for } \Delta T_{L} = 40 \text{ K} \quad (40), \quad (y_{VSL}^{+})_{TEM} = 3.30 Re_{d}^{0.1} \quad \text{for } \Delta T_{L} = 80 \text{ K} \quad (41)$$

$$(y_{VSL}^{+})_{TEM} = 3.65 Re_{d}^{0.1} \quad \text{for } \Delta T_{L} = 100 \text{ K} \quad (42), \quad (y_{VSL}^{+})_{TEM} = 4.00 Re_{d}^{0.1} \quad \text{for } \Delta T_{L} = 120 \text{ K} \quad (43)$$

$$(y_{VSL}^{+})_{TL} = 2.23 Re_{d}^{0.1} \quad \text{for } \Delta T_{L} = 40, 80, 100 \text{ and } 120 \text{ K} \quad (44)$$

6. Nomenclature

С	specific heat, J/kg K	L	heated length, m
c_p	specific heat at constant pressure, J/kg K	L_e	entrance length, m
d	test tube inner diameter, m	$L_{e\!f\!f}$	effective length, m
f_F	fanning friction factor	L_{ex}	exit length, m
G	$=\rho_l u$, mass velocity, kg/m ² s	L_{ts}	test section length, m
h	turbulent heat transfer coefficient,	Nu_d	$=hd/\lambda_l$, nusselt number
	W/m^2K	P	pressure, kPa
I	current flowing through standard	P_{in}	pressure at inlet of heated section, kPa
	resistance, A	P_{ipt}	pressure measured by inlet pressure

$P_{out} \ P_{opt}$	transducer, kPa pressure at outlet of heated section, kPa pressure measured by outlet pressure transducer, kPa	и	between heater inner surface temperature and liquid bulk mean temperature, K flow velocity, m/s
Pr	$=c_p\mu_l/\lambda_l$, Prandtl number	u_{sw}	swirl velocity, m/s
Q	heat input per unit volume, W/m ³	V	volume, m ³
Q_0	initial exponential heat input, W/m ³	w	width of twisted tape, m
q	heat flux, W/m ²	\mathcal{Y}	= H/d =(pitch of 180° rotation)/ d , twist
q_0	initial exponential heat flux, W/m ²		ratio of twisted tape
R_1 to Ra	R_3 resistance in a double bridge circuit, Ω average roughness, μ m	y^+ VSL	$= \left(\frac{f_F}{2}\right)^{0.5} \frac{\rho_l u \delta_{VSL}}{\mu_l}, \text{ non-dimensional}$
Re_d	$=Gd/\mu_l$, Reynolds number		thickness of viscous sub-layer
Re_{sw}	$=\rho_l u_{sw} d/\mu_l$, Reynolds number based on	Z	length, m
	swirl velocity	\boldsymbol{z}	rectangular coordinate, m
Rmax	maximum roughness depth, μm	δ	wall thickness, mm
Rz	mean roughness depth, μm	δ_T	thickness of twisted tape, m
r	radial distance in cylindrical coordinate	δ_{VSL}	= $(\Delta r)_{out}/2$, thickness of viscous sub-
	and test tube radius, m		layer
r_i	test tube inner radius, m	${\cal E}$	emissivity
r_o	test tube outer radius, m	heta	angle in cylindrical coordinate, radian
$(\Delta r)_{out}$		λ	thermal conductivity, W/mK
S	surface area, m ²	μ_l	viscosity, Ns/m ²
T	temperature, K	μ_{w}	viscosity at the temperature of the tube
TEM	analyzed temperature of the outer		wall, Ns/m ²
<i>m</i>	control volume, K	ρ	density, kg/m ³
T_f	liquid temperature, K	τ	exponential period, s
$T_{f,av}$	average liquid temperature, K		-
T_{in}	inlet liquid temperature, K	Subsc	ript
T_L	$=(T_{in}+T_{out})/2$, liquid bulk mean	in	inlet
T	temperature, K	out	outlet
T_{out}	outlet liquid temperature, K	l	liquid
T_s	calculated outlet liquid temperature, K heater inner surface temperature, K	sub	subcooled conditions
t^{S}	time, s	w	wall
ΔT_L	= $(T_s - T_L)$, temperature difference	wnh	with no heating
△1 L	(15-11), temperature difference		

7. Acknowledgments

This research was performed as a LHD joint research project of NIFS (National Institute for Fusion Science), Japan, NIFS05KFRF015, 2010. This research was supported by a Grant-in-Aid for Scientific Research from Japan Society for the Promotion of Science (22560196), 2010.

8. References

- [1] Hata, K., and Noda, N., 2008, "Turbulent Heat Transfer for Heating of Water in a Short Vertical Tube," *Journal of Power and Energy Systems*, **2**, No. 1, pp. 318-329.
- [2] Dittus, F., W., and Boelter, L., M., K., 1930, Univ. Calif. (Berkeley) Pub. Eng., 2, p. 443.

- [3] Nusselt, W., 1931, Der Wärmeaustausch zweischen Wand und Wasser im Rohr, *Forsch. Geb. Ingenieurwes.*, **2**, p. 309.
- [4] Sieder, E. N., and Tate, C. E., 1936, "Heat Transfer and Pressure Drop of Liquids in Tubes," *Ind. Eng. Chem.*, **28**, pp. 1429-1435.
- [5] Petukhov, B. S., 1970, "Heat Transfer and Friction in Turbulent Pipe Flow with Variable Physical Properties," *Advances in Heat Transfer*, New York, Academic Press, pp. 503-564.
- [6] Gnielinski, V., 1976, "New Equations for Heat and Mass Transfer in Turbulent Pipe and Channel Flow," *International Chemical Engineering*, **16**, No. 2, pp. 359-368.
- [7] Hata, K., and Masuzaki, S., 2009, "Twisted-Tape-Induced Swirl Flow Heat Transfer and Pressure Drop in a Short Circular Tube under Velocities Controlled," Proceedings of 13th International Topical Meeting on Nuclear Reactor Thermal Hydraulics, Kanazawa City, Ishikawa Prefecture, Japan, Paper No. N13P1114, pp. 1-15.
- [8] Hata, K., and Masuzaki, S., 2010, "Twisted-Tape-Induced Swirl Flow Heat Transfer and Pressure Drop in a Short Circular Tube under Velocities Controlled," *Nuclear Engineering and Design*, (in press), pp. 1-11.
- [9] Brodkey, R. S., and Hershey, H. C., 1988, *Transport Phenomena*, McGraw-Hill, New York, p. 568.
- [10] Bird, R.B., Stewart, W.E., and Lightfoot, E.N., 1960, *Transport Phenomena*, New York, John Wiley & Sons, p. 85.
- [11] Patankar S.V., 1980, *Numerical Heat Transfer and Fluid Flow*, Hemisphere Pub. Corp., New York.
- [12] Spalding, D.B., 1991, *The PHOENICS Beginner's Guide*, CHAM Ltd., London, United Kingdom.
- [13] Hata, K., and Masuzaki, S., 2010, "Subcooled Boiling Heat Transfer for Turbulent Flow of Water in a Short Vertical Tube," *Journal of Heat Transfer*, Trans. ASME, Series C, **132**, pp. 011501-1-11.
- [14] Hata, K., Shiotsu, M., and Noda, N., 2004, "Critical Heat Fluxes of Subcooled Water Flow Boiling against Outlet Subcooling in Short Vertical Tube," *Journal of Heat Transfer*, Trans. ASME, Series C, **126**, pp. 312-320.
- [15] Hata, K., Komori, H., Shiotsu, M., and Noda, N., 2004, "Critical Heat Fluxes of Subcooled Water Flow Boiling against Inlet Subcooling in Short Vertical Tube," *JSME International Journal*, Series B, 47, No. 2, pp. 306-315.
- [16] Hata, K., Shiotsu, M., and Noda, N., 2006, "Critical Heat Flux of Subcooled Water Flow Boiling for High *L/d* Region," *Nuclear Science and Engineering*, **154**, No. 1, pp. 94-109.
- [17] Hata, K., Shiotsu, M., and Noda, N., 2007, "Influence of Test Tube Material on Subcooled Flow Boiling Critical Heat Flux in Short Vertical Tube," *Journal of Power and Energy Systems*, 1, No. 1, pp. 49-63.
- [18] Hata, K., and Masuzaki, S., 2009, "Subcooled Boiling Heat Transfer in a Short Vertical SUS304-tube at Liquid Reynolds Number Range 5.19×10⁴ to 7.43×10⁵," *Nuclear Engineering and Design*, **239**, pp. 2885-2907.
- [19] Hata, K., and Masuzaki, S., 2010, "Critical Heat Fluxes of Subcooled Water Flow Boiling in a Short Vertical Tube at High Liquid Reynolds Number," *Nuclear Engineering and Design*, **240**, pp. 3145-3157.
- [20] Hata, K., and Masuzaki, S., 2011, "Subcooled Water Flow Boiling Heat Transfer in a Short SUS304-Tube with Twisted-Tape Insert," *Journal of Engineering for Gas Turbines and Power*, Trans. ASME, **133**, pp. 052906-1-11.